Dynamic modelling reveals the separable contributions to achieving correct spindle orientation in a noisy system

AM. Corrigan[†], R. Shrestha[‡], V. M. Draviam[‡] and A. M. Donald*[§]

Keywords: Mitotic Spindle Orientation, Dynamic model, Stochastic simulation

[†]Current address: Laboratory for Molecular Cell Biology and Department of Cell & Developmental Biology, University College London, UK

[‡]Department of Genetics, University of Cambridge, UK

[§]Cavendish Laboratory, Department of Physics, University of Cambridge, UK

Abstract

The mechanisms by which the mammalian mitotic spindle is guided to a predefined orientation through microtubule-cortex interactions have recently received considerable interest, but there has been no dynamic model that describes spindle movements towards the preferred axis in human cells. Here, we develop a dynamic model based on stochastic activity of cues anisotropically positioned around the cortex of the mitotic cell and we show that the mitotic spindle does not reach equilibrium prior to chromosome segregation. Our model successfully captures the characteristic experimental behaviour of noisy spindle rotation dynamics in human epithelial cells, including a weak underlying bias in the direction of rotation, suppression of motion close to the alignment axis, and the effect of the aspect ratio of the interphase cell shape in defining the final alignment axis. We predict that the force exerted per cue has a value which minimizes the deviation of the spindle from the predefined axis. The model has allowed us to systematically explore the parameter space around experimentally relevant configurations, and predict the mechanistic function of a number of established regulators of spindle orientation, highlighting how physical modelling of a noisy system can lead to functional biological understanding. We provide key insights into measurable parameters in live-cells that can help distinguish between mechanisms of microtubule and cortical-cue interactions that jointly control the final orientation of the spindle.

Introduction

During tissue development and homeostasis, the geometry and the position of the constituent cells are important for tissue function (1-3). Cell positioning defects can arise from errors in the process of cell division as the position of the mitotic spindle determines the position of the cleavage plane, and thus determines the size, content and neighbourhood of the two daughter cells (reviewed in (4)). Thus, in a growing or repairing polarised tissue, the orientation of the spindle must be tightly controlled to ensure that each daughter cell is positioned correctly and receives the correct complement of polarity proteins to maintain the function and morphology of the tissue (5, 6). Therefore, knowledge of the mechanisms that orient the spindle is vital to understanding the causes of many developmental disorders, cancers and age-related tissue pathologies.

While the majority of microtubules that emanate from each spindle pole overlap to form the basic structure of the spindle, astral microtubules grow from each pole in all directions (reviewed in (7)). Astral microtubules have long been implicated in spindle centering (8) through forces generated by cytoplasmic motors (9) and compressive forces transmitted to the poles (3, 10-13). The dynamics of spindle positioning in the single cell stage of the *C. elegans* embryo have been modelled, with temporal regulation of cortical pulling forces proposed to explain the centering and subsequent displacement of the spindle, giving rise to an asymmetric first division (14).

In addition to spindle position, correct spindle orientation is critical to ensure robust development. In cells in culture which have no predefined polarity, it has been proposed that the final spindle orientation is determined probabilistically by the distribution of cell-cortex bound structures, generally referred to as cortical cues (15), which form at the site of focal adhesions upon entry into mitosis. In the first model of spindle orientation in human cells, it is suggested that these cues interact with astral microtubules by exerting a pulling force, resulting in a torque that rotates the spindle. Growing cells on geometrically defined micropatterns of the extracellular matrix protein fibronectin controls the localization of focal adhesions to such an extent that the probability distribution of the final spindle orientation can be predicted based on a quantitative model (16). In this model, the angular distribution of cortical cues defines a potential energy landscape, which determines the probability distribution of the spindle angle at equilibrium in the presence of a specified level of Gaussian white noise. The distribution calculated is in dynamic equilibrium in the sense that the overall distribution should not change over time, although spindles are not fixed at the minimum in the potential.

Epithelial cells in culture tend to align their division plane with the short axis of the cell shape during interphase(17). Thus one can equate the preferred spindle axis, corresponding to the minimum of the potential landscape, with the long axis of the cell. In a recent experimental work in human epithelial cells(18), expressing a tubulin marker, the dynamics of spindle rotation were followed and the rotation was found to be noisy, with a small bias in the direction of movement being sufficient to achieve satisfactory final alignment. The dynamic measurements have highlighted additional complexities in spindle movements(18), requiring the model of cortical-cue-driven orientation to be reformulated in terms of the separable contributions to spindle behaviour.

The potential landscape model (16) predicts the equilibrium orientation distribution but not the rotation dynamics, and is in essence a static model. It is important to emphasize that, while implicit in this static model is angular diffusion on a potential gradient, there is only one free parameter – an effective Boltzmann parameter - which is fitted to the final angular distribution of spindles. This single parameter is an aggregate of every process by which spindle rotation is affected and cannot distinguish a defect in final spindle orientation caused by a perturbation to microtubule dynamics,

cortical cue positioning, force exertion or duration of mitosis. Therefore it is highly challenging to unambiguously infer the underlying mechanistic cause for a failure in spindle orientation exclusively on the basis of the final distribution of spindle orientations at the point of cell division.

To understand the time-dependent spindle orientation behaviour, we develop a dynamic model of spindle rotation from nuclear envelope breakdown (NEBD) to anaphase onset. We identify the region in parameter space that recapitulates the behaviour of unperturbed cells in culture and find that the noisy behaviour and two regimes of spindle rotation arise from a weak, orientation-dependent bias in the direction of rotation. By exploring the sensitivity of the observations to parameter perturbations, the dynamic model is able to predict the mechanistic effect of a protein knockdown or drug treatment condition, and thus separate the potential contribution of factors that govern the final orientation of the mitotic spindle. We discuss the implications of our results in the context of recent experimental studies of spindle orientation lesions.

Results

Time-lapse imaging illustrates the strengths of a dynamic model in explaining spindle movements

Our starting point for the dynamic model is the angular distribution of cortical cues on the cortex of the rounded mitotic cell, which, as in the static model, interact in a first-order manner with astral microtubules (see figure S1). In effect, the memory of the interphase cell shape and the long axis must be encoded in this angular distribution. To create a model where dynamics are integral to the behaviour, we assume that each cortical cue has a binary activity profile; inactive cues switch on with a rate proportional to the angular density of microtubules at the cue position, $k_{on} = \kappa \dfrac{\partial \beta}{\partial \theta}$, while active cues switch off with a constant rate k_{off}. While active, cues exert a constant force on the spindle pole that was nearest at the time of activation. The magnitude and duration of the force is condensed into a single parameter, the cue impulse, f_{cue}. Full details of symbols, the dynamic model and simulations are provided in Appendix A.

Stochastic cue activity provides two sources of noise in the number of active cues per frame and the total impulse exerted by a cue before it is deactivated. Additionally, random Brownian noise affects spindle rotation, which we model as Gaussian white noise of variance, σ^2_{noise}. We considered the number of times a cue becomes active during a window of time, and the impulse exerted by the active cue as random variables. Thus for a given spindle orientation, the angular displacement is modelled as a random distribution (see Appendix B) characterized by the mean and standard deviation. The spindle displacement is expressed probabilistically as a stochastic matrix, allowing the evolution of the spindle orientation distribution to be calculated over time (fig S2). This approach allows the dynamics to be calculated at very short times where the magnitude of spindle rotation is small and then extrapolated to experimentally observable timescales where the spindle angle can change continuously throughout the frame interval. Predictions for the rotation bias and speed for a given frame interval were calculated from the stochastic matrix, and were found to be in good agreement with simulated spindles. In the following sections, spindle properties are calculated from the stochastic matrix theory (Appendix B); where individual spindle traces are used, they have been generated from the simulations outlined in Appendix A.

In order for there to be a defined preferential orientation towards which spindles preferentially rotate, the angular distribution of cortical cues must have some anisotropy. We quantify the anisotropy using a two-dimensional order parameter which varies from 0 for purely isotropic cues to 1 for cues positioned on the long axis(19):

$$\rho = 2\left\langle \cos^2 \theta_{cue} \right\rangle - 1 \hspace{6cm} \text{Eq 1}$$

We create a standard anisotropic distribution of cortical cues by uniformly positioning a number of cues around the cortex and adding additional polar cues within 10 degrees of a pre-determined preferred axis, defined as 0°. In the following analysis, the terms long axis and preferred orientation are used interchangeably, and all spindle orientations are measured relative to this axis. The degree of anisotropy can be increased by reducing the number of isotropic cues and increasing the number of polar cues, such that the total number remains constant (see fig S3). The initial cue distribution we use has an order parameter of 0.08.

Parameter space exploration

We first wish to find biologically relevant parameter configurations, which recapitulate the dynamic behaviour observed experimentally. In order to constrain the parameters of the dynamic model, we obtained a large experimental data set (n_{total} = 358, $n_{aspr>1.4}$ = 139) of unperturbed cells from which to extract the characteristic behaviours we aim to understand. We imaged fields of cells at 3 minute intervals and analysed the time lapse movies using our previously developed *spindle3D* software (see Methods), to identify the characteristic experimental behaviour that simulations must capture. All spindle angles are measured relative to the measured interphase long axis of the cell, on the interval [-90, 90] degrees, with zero corresponding to alignment with the long axis. We also refer to the spindle angle as the deviation from the long axis. The long axis is defined by fitting an ellipse to the boundary of the interphase cell shape 15 minutes before nuclear envelope breakdown (NEBD). The initial spindle angle is measured in the first frame after NEBD when a bipolar spindle is first detected. The final spindle angle, also referred to as the division angle, is the angle of the spindle relative to the long axis in the first frame of anaphase, determined from separation of sister chromatids on the metaphase plate. From this experimental dataset, we chose measurable properties which characterise the spindle behaviour - the average division angle, the absolute frame-to-frame rotation speed 45 degrees from the long axis, and the bias in the direction of rotation 45 degrees from the long axis – with which to constrain the parameter space of the dynamic model.

We formed a grid of points covering 2 orders of magnitude of values of the cue activation rate, the impulse exerted per active cue, and the random Brownian noise. The duration of mitosis was approximated by a Gaussian distribution N(μ=30 minutes, σ=2.5 minutes) and a frame interval of 3 minutes was used, matching experimental conditions. The initial spindle orientation was sampled from a uniform distribution, U(0°,90°), consistent with experimental observation (fig S4A), which essentially means that the spindle forms at a random orientation. Figure 1A shows the points which produce output values close to those observed experimentally, which exist in a narrow corridor ranging from low Brownian noise, where a small number of cortical cues exert a large force (left side of 1A), to a regime where a large number of cues exert weak forces and stochasticity is provided by the Brownian noise term (right side of 1A). We choose a point in the middle between these two limiting cases as a standard configuration (κ_0, f_0, σ_0) to represent the unperturbed system for further investigation (black square in figure 1A).

Simulated individual spindle traces bear a strong resemblance to experimental traces, with noisy rotation towards the long axis (figure 1B). The dynamic behaviour is compared between simulation and *in vivo* measurement in figures 1C-G, showing close agreement. The final angular deviation of the spindle from the long axis has a probability distribution peaked around zero (fig 1C), although a
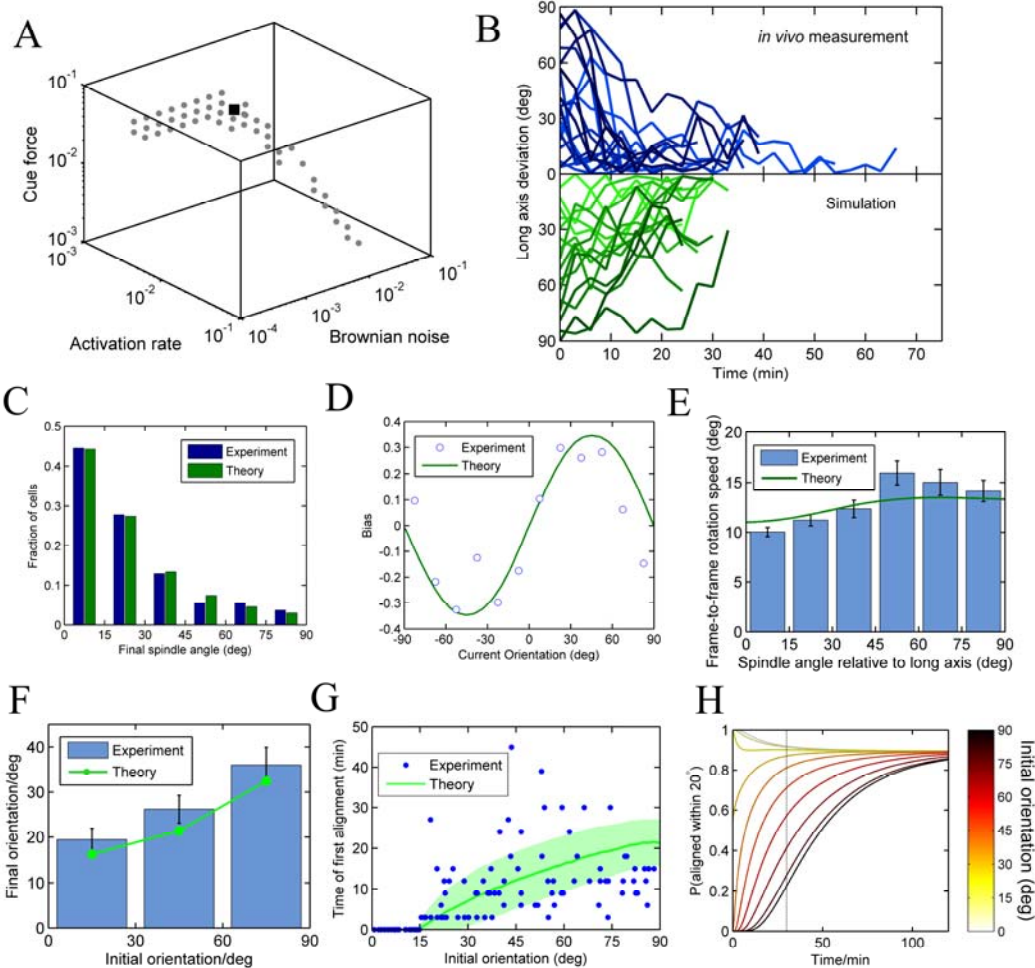
Figure 1 – The dynamic model recapitulates characteristic spindle rotation in cells.

A – Parameter space exploration showing (on-rate, cue force, random noise) triplets which give behaviour quantitatively similar to experiments (circles). Black square denotes parameter set chosen as standard for further study.

B – Traces generated using the parameters, (lower, green), compared with experimental data (upper, blue).

C-G – Comparison of spindle dynamics between experiment (blue) and simulation (green): Final spindle orientation at anaphase onset (C), orientation dependence of directional bias (D) and frame-to-frame speed (E), final orientation as a function of initial orientation (F) and time until first long axis alignment (within 15°) as a function of initial orientation (G). Error bars show SEM and shaded area in G shows standard deviation.

H – Probability of spindle being within 30 degrees of long axis alignment over time, depending on the initial orientation. The vertical dashed line indicates the average time to anaphase onset.

significant fraction of spindles do not reach alignment with the long axis, *in vivo* and in simulations.

Alignment of the spindle with the long axis is achieved by a relatively small bias in the direction of rotation, with spindles slightly more likely to rotate towards the long axis than away (fig 1D). We quantify this directional bias with a value between -1 (all spindles rotating away from long axis) and +1 (all spindles rotating towards long axis), with a value of zero corresponding to spindles equally likely to rotate in either direction, that is, no bias in direction. The bias has a roughly sinusoidal shape and reaches zero when the spindle is aligned with the long axis, or is approximately perpendicular. The speed of spindle rotation (calculated through the frame-to-frame angular displacement) was found to decrease when the spindle was close to the long axis ($p = 8\times10^{-7}$) (fig 1E), which suggests there are two regimes of spindle rotation[18], reducing the likelihood of spindles rotating out of alignment. Orientation-dependent bias in rotation direction and rotation speed suppression both arise naturally in the parameter configurations identified in figure 1A; the suppression of rotation at the long axis is a direct consequence of the variation of bias with orientation (see Supplementary Information). The sinusoidal variation in bias is reproduced *in silico* (figure 1D); the magnitude of the reduction in speed is determined primarily by the anisotropy in the angular distribution of cortical cues, without the need to invoke additional tethering or anchoring once the spindle reaches the long axis.

The initial orientation strongly affects the probability of successful final alignment, with spindles which begin more than 60 degrees from alignment being less likely to end within 20 degrees of the long axis (fig 1F). This failure to align arises because distant spindles require a longer period of time to reach the long axis (fig 1G) and so are less likely to do so successfully before anaphase onset. This implies that the model of dynamic equilibrium in a potential energy landscape does not fully describe spindle dynamics, since the probability of dividing at a certain orientation is not only a function of cortical cue locations but also of initial orientation and time of anaphase onset. This behaviour is captured by the dynamic model, which has important implications for investigating the functional roles of proteins involved in spindle orientation. A defect may arise either from an inability to sense the preferred orientation correctly, or from a problem in rotating the spindle successfully within the time constraint of the duration of mitosis.

The complexity of spindle dynamics means that a perturbation to the system, such as the knocking down of a protein important for spindle movement, may not result straightforwardly in a change in the final division angle. For example in previous work the depletion of MCAK, a kinesin required for microtubule shrinkage, resulted in reduced rotation speeds but did not adversely affect the final spindle alignment and division angle[18]. The good quantitative agreement between in vivo measurement and theory means that the dynamic model is a useful tool to understand spindle behaviour and investigate the mechanisms which are perturbed in the disease state. Therefore, we next use our dynamic physical model to understand the relative importance of system parameters.

Importance of Initial Orientation and Duration of Mitosis

In light of the observation that spindles originating further from alignment take longer to reach the long axis, and are generally less successful in doing so, we next asked how the duration of mitosis influences the likelihood of alignment. It is interesting to note that the bias is very small when the spindle is close to orthogonal to the preferred axis, that is, as far as possible from alignment. Therefore the typical alignment time depends strongly on the initial angular deviation. An important point is that while the spindle assembly checkpoint delays anaphase until all chromosomes are correctly attached to the spindle, there has been no report of a corresponding orientation checkpoint in mammalian cells and it is therefore important that the typical alignment time is

shorter than time until anaphase onset in order that the majority of spindles reach the correct orientation.

Figure 1H shows the probability that a cell has reached alignment as a function of time after NEBD (*x*-axis), for different starting orientations, using the parameter set identified in figure 1A. For non-aligned starting orientations, the probability of having reached alignment increases over time. However spindles which start close to the preferred axis align faster than those which start further away. While this is a fairly intuitive result, it highlights the subtle effect of changing the duration of mitosis. Experimentally, HeLa cells have a duration of mitosis of approximately 30 minutes with a skew-normal distribution (20), which we approximate with a Gaussian distribution. For spindles which start close to the long axis (30-40 degrees), it is very likely that the spindle will reach alignment before anaphase. In contrast, for starting deviations of 70 degrees or greater it is much more likely that a cell will divide before the spindle has had sufficient time to reach alignment. Moreover, a weak perturbation will affect spindles with large initial deviations more strongly than those beginning close to the long axis.

Sensitivity analysis to compare the significance of parameters controlling the final orientation of the spindle

As described above, protein depletion or drug treatment conditions which impair the function of a particular molecular pathway will not always have a direct and unambiguously interpretable effect on the final division angle. To determine the extent to which various input parameters affected the dynamic movements of the spindle, we studied the effect of changing each input parameter in turn by a factor of 2 relative to the unperturbed control configuration. Figure 2A represents the parameter sensitivity as a heatmap, where the size and colour of each circle denotes the relative change in the output property. The properties shown from left to right are the average final deviation from the long axis, the directional bias, the absolute frame-to-frame rotation speed and the magnitude of rotation suppression at the long axis compared to spindles 45 degrees from alignment. The final two columns show the final deviation for spindles which begin within 30 degrees of the long axis (representing retention at the long axis) and outside 60 degrees (representing ability to rotate towards the long axis) respectively. Differences in these two values demonstrate the importance of taking into account the initial spindle orientation. Together the sensitivity measurements provide a 'fingerprint' of the phenotypic effect of a perturbation, which can be compared with experimental protein depletion outcome in cells. It is important to note that the average final deviation increases for all the perturbations shown in figure 2A, meaning the division angle distribution alone is unable to distinguish the affected parameter.

Figure 2B shows the effect of changing the degree of polarization in the angular cue distribution, characterised by the order parameter. The rotation speed (upper panel) for spindles far from alignment (>30 degrees, blue circles) increases and the speed close to the long axis (<30 degrees, black squares) shows a small decrease. Overall alignment with the long axis is improved for highly polarized distributions (central panel, fig 2B) both by increasing the speed of rotation when far from the long axis, and by reducing the rate of rotation once alignment has been achieved. A likely candidate for an experimental change in the cue order parameter is the aspect ratio of the interphase cell shape, which is studied below.

Force exerted by cortical cues determines alignment success

The sensitivity analysis revealed that the average force exerted by each cue does not have a straightforward effect on the probability of alignment. To investigate this further, we varied the

force exerted per cue over two orders of magnitude, holding the other parameters, including the random noise, constant (figure 2C). Interestingly, as the force is increased above the standard value, f_0, alignment success decreases as the effect of a single cue activation is sufficient to move the spindle away from the long axis (bottom panel). This gives rise to an optimal cue force at which spindle deviation from the long axis at the point of division is minimal. The magnitude of the cue force has two opposing effects: it must be large enough to overcome the noise in the system and
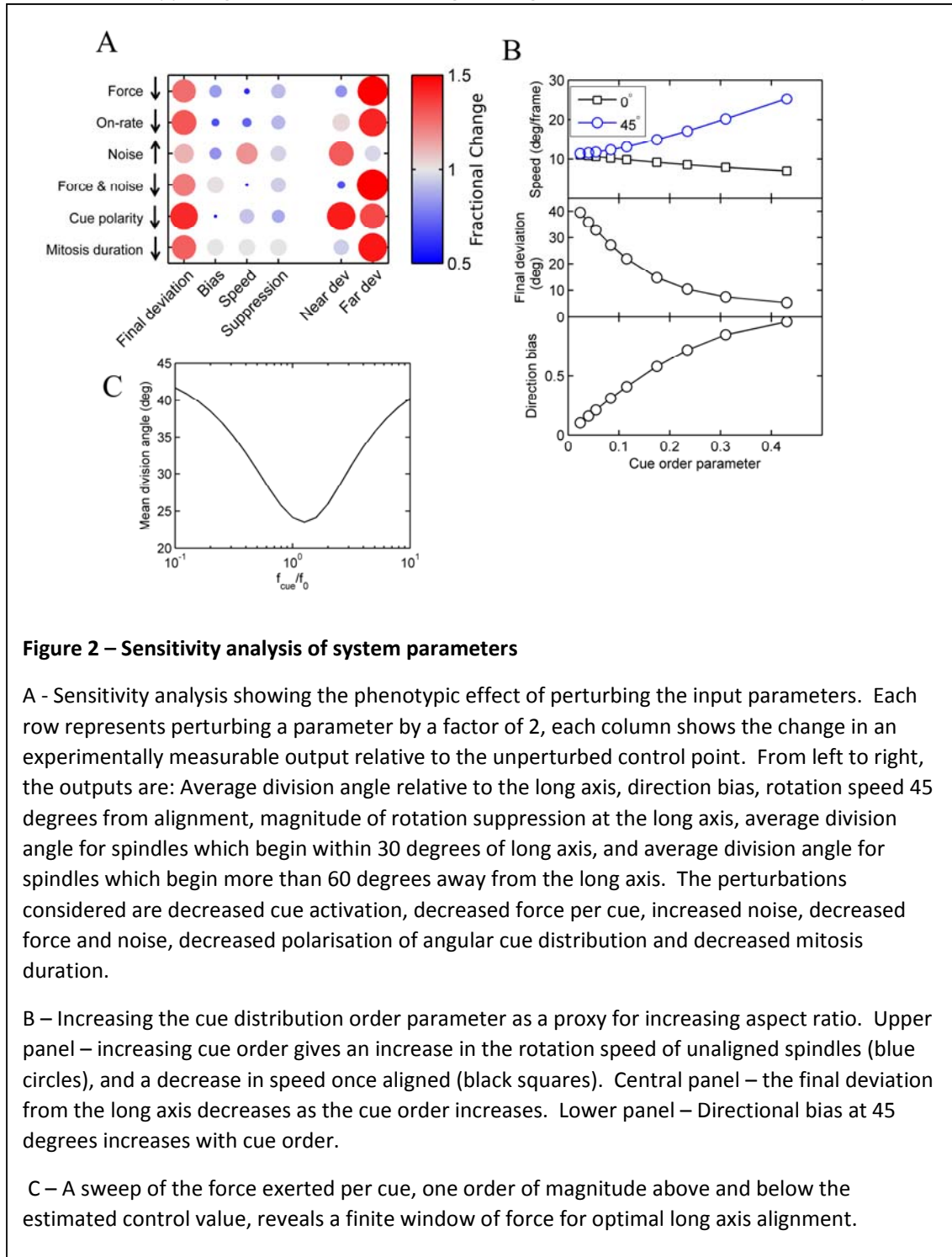
Figure 2 – Sensitivity analysis of system parameters

A - Sensitivity analysis showing the phenotypic effect of perturbing the input parameters. Each row represents perturbing a parameter by a factor of 2, each column shows the change in an experimentally measurable output relative to the unperturbed control point. From left to right, the outputs are: Average division angle relative to the long axis, direction bias, rotation speed 45 degrees from alignment, magnitude of rotation suppression at the long axis, average division angle for spindles which begin within 30 degrees of long axis, and average division angle for spindles which begin more than 60 degrees away from the long axis. The perturbations considered are decreased cue activation, decreased force per cue, increased noise, decreased force and noise, decreased polarisation of angular cue distribution and decreased mitosis duration.

B – Increasing the cue distribution order parameter as a proxy for increasing aspect ratio. Upper panel – increasing cue order gives an increase in the rotation speed of unaligned spindles (blue circles), and a decrease in speed once aligned (black squares). Central panel – the final deviation from the long axis decreases as the cue order increases. Lower panel – Directional bias at 45 degrees increases with cue order.

 C – A sweep of the force exerted per cue, one order of magnitude above and below the estimated control value, reveals a finite window of force for optimal long axis alignment.

rotate the spindle to the long axis, but if it is too large then fluctuations in the stochastic cue activity prevent the spindle remaining aligned. Thus there exists a window of cue force magnitude values where the spindle rotation speed is fast enough to reach alignment before anaphase, but the force is small enough that the system is not dominated by the stochasticity of the cue activity.

Importance of direction bias and rotation speed in distinguishing physical mechanisms that control final spindle alignment

Finally, we take a panel of experimental perturbations that are known to have an effect on the final orientation of the spindle and examine their dynamic phenotypes. The perturbations studied are RNAi-mediated depletion of LGN, treatment with a microtubule pausing agent, 2ME2 (18), comparing low aspect ratio cells with high, and synthetically halving the duration of mitosis. The consequence of LGN depletion and 2ME2 treatment in disrupting the spindle alignment with the long-axis of the cell has been presented previously (18); here we provide a novel interpretation in terms of the dynamic model. Figure 3A shows the dynamic 'fingerprint' for RNAi mediated depletion of LGN, and for treatment with the drug 2ME2 compared with the respective control treated cells. Also shown in figure 3A is data for low aspect ratio control cells (<1.3) compared with more elongated cells, and an artificial shortening of the mitosis duration, constructing by considering only the first half of the experimental spindle angle data. The phenotypic maps can be compared with the sensitivity maps of figure 2A to predict the parameter(s) that are perturbed by the treatment. Comparing low aspect ratio cells with high suggests that the interphase cell shape is linked to the polarisation in the angular distribution of cue locations, as may be expected. Intuitively, shortening the mitosis duration does not affect the speed of rotation or bias, but adversely affects the alignment success of spindles originating more than 60 degrees from the long axis. This also suggests that the system parameters do not change significantly throughout mitosis. LGN depletion and 2ME2 treatment have similar phenotypes, and are considered in more detail in figure 3B. As with the sensitivity analysis (fig 2A), the change in final spindle deviation is similar for all perturbations considered, and therefore measuring only the distribution of final spindle orientation yields very little insight into the physical mechanisms being disrupted.

As described above, it is not trivial to unambiguously infer the parameter which has been affected for LGN depleted or 2ME2 treated cells because the fingerprints for cortical-cue force and activation rate are similar. By considering the effect on the bias and speed together we can predict the source of the perturbation. As shown in figure 3B, reducing the force exerted per cue affects the rotation speed to a greater degree than the directional bias; whereas reducing the cue activation rate affects the bias more strongly than the speed. Analysed in this way, we predict that LGN depletion (fig 3B, red circle) results in a reduction in the force exerted by the cortical cues, while 2ME2 treatment affects the on-rate. Consistent with this interpretation, LGN depletion does not affect the final deviation of spindles starting close to alignment (near dev., fig 3A) in agreement with the force perturbation in figure 2A. Thus the dynamic model allows us to distinguish between mechanisms that jointly govern the movements of the spindle towards its predefined final alignment axis.
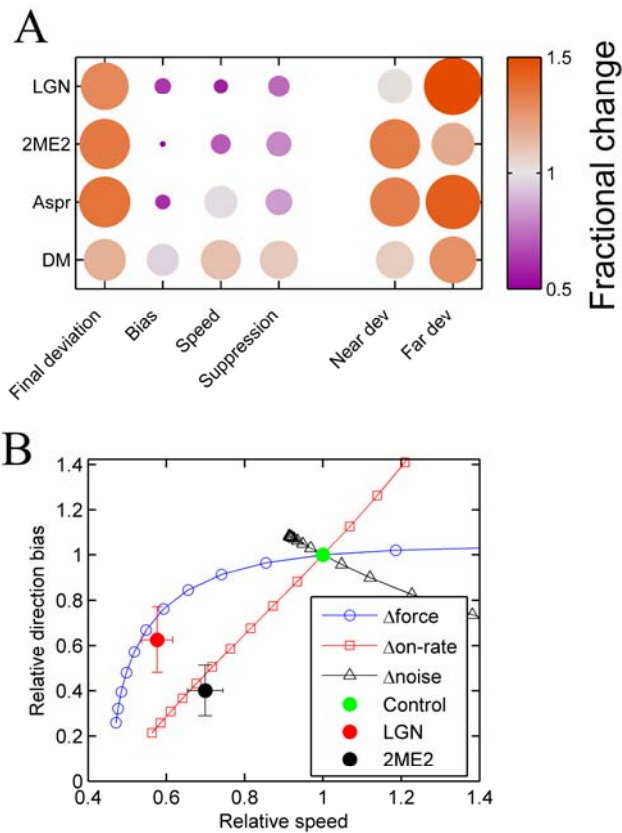
Figure 3 – Interpreting the consequence of molecular defects.

A – heatmap showing the effect of dynamic measurements from a range of experimental treatments. From top to bottom, the experimental perturbations are: LGN protein depletion, 2ME2 drug treatment, low aspect ratio unperturbed control cells (Aspr), and artificially halved mitosis duration (DM). (see text).

B – decreasing cue force (Δforce) and decreasing cue activation (Δon-rate) have similar phenotypic 'fingerprints' (figure 2A). Simultaneously considering the changes in bias (*y*-axis) and speed (*x*-axis) can help to distinguish these perturbations relative to the estimated control point (green circle). Decreasing the force (blue circles) is predicted to affect the speed to a greater extent than the bias – the LGN depletion phenotype (red circle) is best explained by this perturbation. In contrast, treatment with 2ME2 (black circle) decreases the directional bias more strongly than the speed, consistent with a decrease in the cue activation rate (red squares).

Discussion

In this paper, we have constructed a dynamic model of mitotic spindle rotation, considering the physical interaction between the astral microtubules of the spindle and stochastically active cortical cues to understand spindle behaviour in a time-dependent manner. The model captures the characteristic dynamic behaviour of the spindle – weak bias in the direction of rotation, strong dependence on initial orientation – and can be directly compared with experimental data from time-lapse movies of human epithelial cells to reveal the mechanistic function of the molecular players that control spindle orientation.

We have simulated the behaviour for the case where each cortical cue exerts a fixed force and the preferred axis is defined by the anisotropy in the angular distribution of the cues. Equivalently, there may instead be anisotropy in the cue activity, either through the force exerted or the activation rate. It has been reported that cell stretching can change the preferred axis during mitosis (21), suggesting a modulation of activity by retraction fibre tension can override the previous axis of anisotropy. A microtubule length dependence could be added to the activation rate, through the astral microtubule density (equation A-2 in Appendix A), or exerted force terms, by assuming an exponential distribution of lengths. This might be expected to reduce the speed of rotation once the spindle is aligned, since distant cortical cues will contribute less to spindle rotation. The potential for cortical cues to modulate microtubule length is discussed further below.

Our model highlights the importance of the initial spindle orientation in determining the likelihood of successful alignment. We showed experimentally how the final deviation depends strongly on the initial angle (fig 1F), in agreement with *in silico* predictions. Therefore, in cell types where correct orientation is critically important, centrosome positioning may be employed before nuclear envelope breakdown to 'pre-orient' the spindle and ensure that the orientation process is fast enough (3).

In our model we consider only cortical forces acting on astral microtubules to generate a systematic torque on the spindle. Additionally, cytoplasmic motors may pull on the spindle with a force that is a function of the microtubule length (3, 12). In this way, an asymmetry in astral microtubule length would generate rotation. However, in the conditions we have considered in human cells, where the spindle is in the centre of a rounded cell, cytoplasmic forces will be absorbed into the random noise term.

We found that there is an optimal value of the cue force to obtain good alignment with the long axis, above which stochasticity in cue activity causes the spindle to be rotated away from the long axis, a feature which is not predicted by the static model. Experimental work has previously suggested that force-generating dynein must be recruited to the cortex at the appropriate level to result in successful orientation (22). The experimental rotation speed is consistent with a cue force close to this optimal value. This is an illustration of the complex phenotypic output of a perturbation; increases in activity and not only protein knockdowns can have deleterious effects. By performing a corresponding sweep in the value of the Brownian random noise, we found that reducing the Brownian noise *increased* the alignment time and typical deviation for spindles which started far from alignment (figure S5B). Potentially, some noise is beneficial in moving spindles away from perpendicular orientations where the net cue torque is small, sacrificing perfect alignment with the preferred axis in favour of achieving reasonable alignment for the majority of cells within the tight time constraint before anaphase onset. In support of this hypothesis, such sacrifice in perfect alignment with the preferred axis is in fact observed in vivo tissues where the spindle is orientated within 40 degrees of the predefined axis (23, 24).

By comparing the shift in dynamic properties relative to unperturbed cells, we are able to predict how the system parameters are changed when an experimental perturbation is applied. This dynamic fingerprint can distinguish between changes to the activation rate, the force exerted per cue, the Brownian noise and the angular distribution of cortical cues, something which the static final spindle angle distribution cannot. We inferred that depletion of LGN caused the cue force to be reduced, consistent with a role for LGN in recruiting dynein, a minus-end directed force-generating motor protein, to the cortex to interact with astral microtubules (18, 25-27). Treatment with 2ME2 led to a reduction in the cue activation rate, as may be expected from a drug which suppresses microtubule dynamics (28). The ability to predict the mechanistic effect of a genetic knockdown is a significant strength of the dynamic model.

For cells in culture, the precise distribution of cortical cues is not known and is instead approximated as a polarized non-uniform distribution characterized by a two-dimensional order parameter. In this respect, measuring the spindle dynamics of cells cultured on adhesive micropatterns may allow more reproducible shapes and cue distributions to be studied. As described above, a proportion of the Brownian random noise arises from astral microtubules which are not interacting with the cortical cues. These microtubules are thought to exert a compressional pushing force when they are sufficiently long to reach the cortex, and have been implicated in maintaining the position of the spindle at the centre of the cell(10). Mathematically there is no distinction between a pulling force and the absence of a pushing force. Without a precise biochemical mechanism for the MT-cue interaction, it is interesting to speculate that a cue may operate by stalling or depolymerizing microtubules thereby removing the pushing force at specific non-uniform locations on the cortex. The cue activity 'lifetime' would then be defined by the time for the depolymerizing microtubule to be rescued and reach the cortex again, which might be significantly greater than the lifetime expected for a direct molecular interaction. Also, a single cue would be able to have a simultaneous effect on many microtubules, increasing the potential total force per cue beyond the pN range typical of MT-mediated forces. An alternative mechanism by which cortical cues could modulate the astral microtubule pushing force is by influencing the local membrane rigidity (29, 30). In this scenario an active cue reduces the membrane stiffness such that an elongating astral microtubule deforms the cortex to a greater degree and results in a reduced compressive force being transmitted to the spindle pole. Bundling of microtubules may also be a mechanism by which the lifetime or force produced by a cortical interaction can be increased beyond those of a single, dynamically-unstable microtubule.

Regardless of the precise mechanism of action of cortical cues, the processes of spindle orientation and spindle location or centering are inescapably linked, and future work to combine the two phenomena in a single model will shed further light on the mechanisms at work. We have presented a dynamic framework for studying the interplay of factors which determine the degree of alignment of the mitotic spindle to a cell-polarity-defined preferred axis. Our approach of quantitative live imaging combined with theory and simulation will find use in investigating the mechanics of spindle orientation and the protein regulators involved in cells grown in culture, as well as cells grown on adhesive micropatterns and within the context of tissues and metastatic cells.

Appendices

Appendix A – Detailed description of Dynamic Model

The dynamic model makes the basic assumption that spindle orientation is controlled, at least in part, by cortical cues which are fixed in number and position over time. The current proposal for how the cues influence the spindle is through an interaction with the astral microtubules which are connected to one spindle pole or the other. More generally, we assume that the cues exert a pulling force on the nearest spindle pole, and thereby generate a torque on the spindle, without specifying the precise mechanism of this action.

Typically we represent stochastic cue deactivation with an exponentially distributed lifetime $\tau_{cue} = (k_{off})^{-1}$. An active cue exerts a fixed pulling force on the spindle pole which was nearest at the time of activation along the line between the cue and the pole, while an inactive cue does not influence the spindle. The pole being influenced by the cue is chosen as the nearest to the cue at the time of activation; the same pole is influenced until the cue deactivates, even if the other pole becomes closer during this time. Cue switching and rotation of the spindle is calculated over a very small time increment, typically 0.2s. The precise value of the time increment chosen does not influence the results observed as long as the increment is much shorter than any characteristic timescale in the system.

The angular impulse acting on the spindle in each increment is calculated by summing the force vectors of active cues combined with a random noise torque, and each cue has a probability of switching per time increment. In the low Reynolds number, viscous regime within the cell, the angular displacement per time step is proportional to the calculated torque, and so we define the force exerted per cue and noise directly in terms of the resultant angular velocity of the spindle, incorporating the rotational friction coefficient of the spindle into the force and noise terms. Therefore it is important to note that if the rotational drag coefficient were to change, through either the shape of the spindle or the viscosity of the cytoplasm, the cue force and noise terms would need scaling accordingly. Also, while the magnitude of the force exerted by a cue is constant, the value of the torque will depend on the current position of the spindle as well as the configuration of active cues.

When the cell rounds for mitosis, we make the assumption that the angular position of each cortical cue from the centre of the cell does not change (see fig S2). The angles of the cortical cues are shown in figure S5, with an axis of anisotropy which defines the preferred spindle axis

A cue is activated by interacting with a microtubule, therefore we assume that the rate of an 'off' cue switching on is proportional to the angular density of astral microtubules,

$$k_{on} = \kappa \frac{d\beta}{d\theta}\bigg|_{\theta_i}$$ Eq (A1)

Where, from geometric considerations:

$$\frac{d\beta}{d\theta}\bigg|_{\theta_i} = \frac{1 - \frac{a}{R}\cos(\theta_i - \phi)}{1 - \frac{2a}{R}\cos(\theta_i - \phi) + \frac{a^2}{R^2}}$$ Eq (A2)

The partial differential captures the change in angle from the spindle pole due to a small movement around the cortex, and hence reflects the density of microtubules experienced locally at cortex angle θ_i. Equivalently, locations on the cortex which are further from the spindle pole have a lower density of microtubules. The angles β, φ and θ are defined as shown in figure S2B. The effective on-rate varies from being maximal where the microtubules are densest close to a spindle pole to a minimum when they are perpendicular to the spindle angle. Where the value of an on-rate is referred to explicitly, for example when using the analytical approximation described below, we refer to the prefactor κ. We assume that the rate of switching off is constant per time step, which means that the lifetime of an active cue has an exponential probability distribution with a mean duration $\tau_{cue}=1/k_{off}$.

For our simulations, we define a small and fixed time step, t_{inc}, during which the probability of transitions and the movement of the spindle is evaluated. The time step typically chosen is 0.2 seconds, orders of magnitude smaller than our typical imaging time step for experimental comparison. The method of small frame increments was chosen above a purely Monte Carlo approach since the on-rates and thus the probabilities of cue transitions are functions of the current spindle orientation, which varies continuously.

While a cue is active, it exerts a fixed force along the line between the cue and one spindle pole. The pole being influenced by the cue is chosen as the nearest to the cue at the time of activation; the same pole is influenced until the cue deactivates, even if the other pole becomes closer during this time. Thus while the magnitude of the force exerted by a cue is constant, the value of the torque will depend on the current position of the spindle as well as the configuration of active cues. The total vector force on each pole is summed and the torque calculated using the vector product with the axis of the spindle. Gaussian white noise is added to the torque before it is used to update the spindle position.

In updating the spindle orientation for the next time point, we assume that the angular velocity is constant throughout the short time step. At each time point the process is repeated: within a time step there is a probability that each active cue will be deactivated. Correspondingly, each inactive cue has a probability of switching on that is also a function of the angular density of microtubules (see figure S1).

Appendix B – Representing spindle movement as a Gaussian random variable

In this appendix we calculate the mean and variance of the random variable which describe the frame-to-frame spindle rotation. Since the angular inertia of the spindle is an unknown quantity, we make the assumption that rotation rates are in the viscous regime and express the impulse exerted per cue directly in terms of the resulting angular displacement divided by the spindle half-length, a. It is therefore important to note that perturbations which change the spindle size or rotational drag coefficient will scale the effective cue impulse parameter accordingly. We first calculate the expectations of mean and variance of the spindle displacement for a small patch of the cortex an angle ϑ from the spindle, and then sum over the whole cortex using standard rules for the combination of random variables.

If astral microtubules are assumed to emanate from each spindle pole, uniformly in all directions, the angular density of microtubules for the cortex at angle theta is given by:

$$\rho_{MT}(\theta) = \frac{d\beta}{d\theta} = \frac{1 - a\cos\theta}{1 - 2a\cos\theta + a^2} \qquad \text{Eq A-2}$$

The equation above for astral microtubule density does not include a microtubule length-dependence factor; this could be incorporated by using the distance from pole to cortex, $|\mathbf{l}|$, and assuming an exponential length distribution.

At a point on the cortex an angle ϑ from the spindle angle, the vector from spindle pole to cortex is given by (see fig S2B):

$$\mathbf{l} = \mathbf{r} - \mathbf{a}$$

$$\begin{pmatrix} l_x \\ l_y \end{pmatrix} = \begin{pmatrix} \cos\theta - a \\ \sin\theta \end{pmatrix}$$

Only when the force vector is perpendicular to the spindle axis is the full cue impulse, f_{cue}, imparted to the spindle. For the cortex at angle theta, the attenuated angular impulse, α, is calculated using the geometry shown in figure S2B as:

$$\alpha = f_{cue}\sin\beta = \frac{f_{cue}\sin\theta}{\sqrt{1+a^2-2a\cos\theta}} \qquad\qquad \text{Eq A-1}$$

The number of cue contributions from the patch of cortex has a Poisson distribution with mean λ, where λ is the product of the number of cortical cues in the patch, the frame interval, the activation rate and the density of astral microtubules:

$$\lambda = n_{cue}(\psi)t_{frame}\kappa_{on}\rho_{MT}(\psi)$$

For combination of random variables, we can use the Gaussian approximation of a Poisson distribution. The cortical cues at angle ϑ each exert an impulse α on the spindle, meaning the distribution of angular impulse from the patch of cortex is given by:

$$\text{Spindle displacement} = N\left(\mu = \alpha\lambda, \sigma^2 = \alpha^2\lambda + t_{frame}\sigma_{noise}^2\right)$$

The mean and variance of the total spindle displacement distribution is found by integrating over the whole cortex:

$$\mu_{tot}(\phi) = f_{cue}t_{frame}\kappa_{on}\int_{\theta=-\pi/2}^{\theta=\pi/2} n_{cue}(\theta+\phi)\frac{\sin\theta(1-a\cos\theta)}{\left(1+a^2-2a\cos\theta\right)^{3/2}}d\theta$$

$$\sigma_{tot}^2(\phi) = t_{frame}\sigma_{noise}^2 + f_{cue}t_{frame}\kappa_{on}\int_{\theta=-\pi/2}^{\theta=\pi/2} n_{cue}(\theta+\phi)\frac{\sin^2\theta(1-a\cos\theta)}{\left(1+a^2-2a\cos\theta\right)^2}d\theta \qquad \text{Eq A-3}$$

For discrete cue locations,

$$n_{cue}(\psi) = \sum_j \delta(\psi-\psi_j),$$ giving:

$$\mu_{tot}(\phi) = t_{frame}\kappa_{on}\sum_j \frac{\sin\theta_j(1-a\cos\theta_j)}{\left(1+a^2-2a\cos\theta_j\right)^{3/2}}, \quad where \quad \theta_j = \psi_j - \phi$$

$$\sigma_{tot}^2(\phi) = t_{frame}\sigma_{noise}^2 + t_{frame}\kappa_{on}\sum_j \frac{\sin^2\theta_j\left(1 - a\cos\theta_j\right)}{\left(1 + a^2 - 2a\cos\theta_j\right)^2}$$

<div style="text-align:right">Eq A-4</div>

Thus from the angular positions of the cortical cues relative to the spindle we calculate the mean and variance of the rotational displacement. We express the result as a stochastic matrix, M:

$$M_{ij} = P\left(\phi(t + t_{inc}) = \phi_j \mid \phi(t) = \phi_i\right),$$

breaking the interval [-90,90] degrees into 720 bins. The stochastic matrix allows the evolution of a spindle angle distribution to be calculated over time, and allows the dynamics to be calculated at a very short timescale, t_{step}, and extrapolated to give the spindle displacements at typical frame interval, t_{frame}, by raising the matrix to the appropriate power:

$$\mathbf{M_{frame}} = \mathbf{M}^{t_{frame}/t_{inc}}$$

Rotation statistics such as the bias in the direction of rotation and the absolute speed of rotation are calculated directly from the probability distribution of spindle displacements as a function of angle, ie the columns of $\mathbf{M_{frame}}$:

$$M_{frame}^i = P\left(\phi(t + t_{frame}) \mid \phi(t) = \phi_i\right)$$

A stochastic matrix has at least one eigenvalue of value 1, whose corresponding eigenvectors describe the equilibrium spindle orientation distributions (such that the distribution will be unchanged after multiplication by **M**). Furthermore, we can specify a starting angle distribution, $\mathbf{v_0}$, and using the matrix calculate the distribution at the time of division as:

$$\mathbf{v_{div}} = \mathbf{M}^{DM/t_{inc}}\mathbf{v_0}$$

A probabilistic duration of mitosis (DM) is incorporated by summing over the duration distribution:

$$\mathbf{v_{div}}(\phi) = \sum_x p(DM = x)(\mathbf{M})^{x/t_{frame}}\mathbf{v_0}$$

<div style="text-align:right">Eq A-5</div>

Currently, the force is used only to calculate the torque acting around the centre of the spindle; lateral forces are assumed not to displace the spindle away from the centre of the cell. If a length-dependent pushing force was incorporated for astral microtubules not interacting with cortical cues, models for spindle orientation and spindle *positioning* could be combined, to evaluate the extent to which a defect in spindle centering could also induce misorientation.

In our study the number of cues was kept fixed at 60, a value which was chosen to be slightly smaller than that used by Thery et al. in modelling the division angle of cells adhered to fibronectin patterns(16). The important variable in determining the dynamic behaviour is the number of active cues per frame, which is determined by the total number of cues, N, the cue activation rate, κ, and the frame interval. Therefore to a good approximation an increase in the number of cues is equivalent to an increase in the activation rate. A secondary effect of increasing the cue number not considered in this study is that the cell shape is more accurately represented by the distribution of cues.

A striking observation from experimental measurements is the high level of noise present in spindle rotation. For cells of uncontrolled shape in culture, alignment with the long axis is accomplished with a relatively small bias in the direction of rotation. Regarding the origin of the high level of noise in this system, we propose three sources which contribute to the high level of noise. Firstly, stochasticity in the cue activity means that the number of cues which act to move the spindle within a frame interval is stochastic, and so even if the number of cues pulling towards the preferred axis outnumber those pulling away there is a non-zero probability that the spindle will move away from alignment in a given frame. This source of noise was considered in our analytical approximation of the dynamic model. The second noise source arises from a probabilistic lifetime of cue activity. In our system, we assumed that there was a single rate-limiting step for cue activation and deactivation, giving an exponential active cue lifetime distribution. This adds a further level of uncertainty to the total torque and is calculated in Appendix C. The final source of noise is a cue-extrinsic Brownian noise term, defined as a Gaussian whose width is determined by the magnitude of all the additional torques acting on the spindle. As well as molecular collisions, this term includes fluctuations in the forces exerted on the spindle by astral microtubules which are pushing against the cortex rather than interacting with a cue.

Appendix C – Incorporating stochastic cue activity lifetimes

We wish to calculate the probability distribution of the total impulse produced by a Poisson distribution of active cues. Each active cue produces a constant force for a duration of time defined probabilistically by an exponential distribution. This means that the impulse exerted by each cue is a value sampled from the same exponential distribution, so that the total impulse from k cues is a hypoexponential distribution, *H(f,k)*, with mean *fk* and variance f^2k. In our notation *H(f,k)* represents the sum of *k* exponential distributions, each with mean *f*.

If we now consider the case when the number of active cues has a Poisson distribution with parameter λ, the overall distribution is a mixture of hypoexponential distributions, where the mixture coefficients are the Poisson probabilities for the number of active cues. The distribution itself is non-trivial, however the mean and standard deviation can be calculated:

$$\langle X \rangle = \int_0^\infty x p(x) dx$$

$$= \int_0^\infty x \sum_{j=0}^\infty C_j H(f,j) dx$$

$$= \sum_{j=0}^\infty C_j \int_0^\infty x H(f,j) dx$$

$$= \sum_{j=0}^\infty C_j \langle H(f,j) \rangle$$

$$= \sum_{j=0}^\infty C_j f j$$

$$= f \langle C \rangle$$

$$= f \lambda$$

In the equations above, C_j are the Poisson probabilities *P*(number of active cues = *j*).

Therefore the mean impulse is unchanged by incorporating exponential activity lifetimes.

Similarly for the variance:

$$\langle X^2 \rangle = \int_0^\infty x^2 p(x) dx$$

$$= \sum_{j=0}^\infty C_j \int_0^\infty x^2 H(f,j) dx$$

$$= \sum_{j=0}^\infty C_j \langle H^2(f,j) \rangle$$

$$= \sum_{j=0}^\infty C_j (j + j^2) f^2$$

$$= f^2 \sum_{j=0}^\infty C_j j + f^2 \sum_{j=0}^\infty C_j j^2$$

$$= f^2 \lambda + f^2 (\lambda + \lambda^2)$$

$$= f^2 (\lambda^2 + 2\lambda)$$

Where above we have used the definition of variance:

$$\mathrm{Var}[C] = \langle C^2 \rangle - \langle C \rangle^2,$$

$$\lambda = \sum_j C_j j^2 - \lambda^2$$

$$\sum_j C_j j^2 = \lambda + \lambda^2$$

Therefore the variance of the overall distribution is:

$$\mathrm{Var}[X] = \langle X^2 \rangle - \langle X \rangle^2$$

$$\mathrm{Var}[X] = f^2 (\lambda^2 + 2\lambda) - (f\lambda)^2$$

$$\mathrm{Var}[X] = 2 f^2 \lambda$$

The variance of the total impulse is increased by a factor of 2 due to the exponential lifetime of cue activity, compared with fixed cue impulses and only Poisson variance in cue number.

Author Contributions

AMC, VMD and AMD designed research and wrote the paper, AMC developed theory and simulations, AMC and RS performed experimental work.

References

1.   Minc, N., and M. Piel. 2012. Predicting division plane position and orientation. Trends in cell biology 22:193-200.

2.   Morin, X., and Y. Bellaiche. 2011. Mitotic spindle orientation in asymmetric and symmetric cell divisions during animal development. Developmental cell 21:102-119.

3.   Wuhr, M., E. S. Tan, S. K. Parker, H. W. Detrich, 3rd, and T. J. Mitchison. 2010. A model for cleavage plane determination in early amphibian and fish embryos. Current biology : CB 20:2040-2045.

4.   Chin, H. M., K. Nandra, J. Clark, and V. M. Draviam. 2014. Need for multi-scale systems to identify spindle orientation regulators relevant to tissue disorganization in solid cancers. Frontiers in physiology 5:278.

5.   Kulukian, A., and E. Fuchs. 2013. Spindle orientation and epidermal morphogenesis. Philosophical transactions of the Royal Society of London. Series B, Biological sciences 368:20130016.

6.   Gillies, T. E., and C. Cabernard. 2011. Cell division orientation in animals. Current biology : CB 21:R599-609.

7.   Tamura, N., and V. M. Draviam. 2012. Microtubule plus-ends within a mitotic cell are 'moving platforms' with anchoring, signalling and force-coupling roles. Open biology 2:120132.

8.   Hamaguchi, M. S., and Y. Hiramoto. 1986. Analysis of the Role of Astral Rays in Pronuclear Migration in Sand Dollar Eggs by the Colcemid-Uv Method. Dev Growth Differ 28:143-156.

9.   Kimura, A., and S. Onami. 2010. Modeling microtubule-mediated forces and centrosome positioning in Caenorhabditis elegans embryos. Methods in cell biology 97:437-453.

10.   Grill, S. W., J. Howard, E. Schaffer, E. H. Stelzer, and A. A. Hyman. 2003. The distribution of active force generators controls mitotic spindle position. Science 301:518-521.

11.   Laan, L., N. Pavin, J. Husson, G. Romet-Lemonne, M. van Duijn, M. P. Lopez, R. D. Vale, F. Julicher, S. L. Reck-Peterson, and M. Dogterom. 2012. Cortical dynein controls microtubule dynamics to generate pulling forces that position microtubule asters. Cell 148:502-514.

12.   Minc, N., D. Burgess, and F. Chang. 2011. Influence of cell geometry on division-plane positioning. Cell 144:414-426.

13.   Zhu, J., A. Burakov, V. Rodionov, and A. Mogilner. 2010. Finding the cell center by a balance of dynein and myosin pulling and microtubule pushing: a computational study. Molecular biology of the cell 21:4418-4427.

14.   Kimura, A., and S. Onami. 2007. Local cortical pulling-force repression switches centrosomal centration and posterior displacement in C. elegans. The Journal of cell biology 179:1347-1354.

15.   Thery, M., V. Racine, A. Pepin, M. Piel, Y. Chen, J. B. Sibarita, and M. Bornens. 2005. The extracellular matrix guides the orientation of the cell division axis. Nat Cell Biol 7:947-U929.

16.   Thery, M., A. Jimenez-Dalmaroni, V. Racine, M. Bornens, and F. Julicher. 2007. Experimental and theoretical study of mitotic spindle orientation. Nature 447:493-U496.

17.   Hertwig, O. 1884. Das problem der befruchtung und der isotropie des eies. eine theorie der vererbung. Jena. Z Med. Naturwiss. 18:276-318.

18.   Corrigan, A. M., R. L. Shrestha, I. Zulkipli, N. Hiroi, Y. Liu, N. Tamura, B. Yang, J. Patel, A. Funahashi, A. Donald, and V. M. Draviam. 2013. Automated tracking of mitotic spindle pole positions shows that LGN is required for spindle rotation but not orientation maintenance. Cell cycle 12:2643-2655.

19.   Mercurieva, A. A., and T. M. Birshtein. 1992. Liquid-Crystalline Ordering in 2-Dimensional Systems with Discrete Symmetry. Makromol Chem-Theor 1:205-214.

20.   Meraldi, P., V. M. Draviam, and P. K. Sorger. 2004. Timing and checkpoints in the regulation of mitotic progression. Developmental cell 7:45-60.

21.   Fink, J., N. Carpi, T. Betz, A. Betard, M. Chebah, A. Azioune, M. Bornens, C. Sykes, L. Fetler, D. Cuvelier, and M. Piel. 2011. External forces control mitotic spindle positioning. Nat Cell Biol 13:771-778.

22. Kotak, S., C. Busso, and P. Gonczy. 2012. Cortical dynein is critical for proper spindle positioning in human cells. The Journal of cell biology 199:97-110.

23. Lechler, T., and E. Fuchs. 2005. Asymmetric cell divisions promote stratification and differentiation of mammalian skin. Nature 437:275-280.

24. Saadaoui, M., M. Machicoane, F. di Pietro, F. Etoc, A. Echard, and X. Morin. 2014. Dlg1 controls planar spindle orientation in the neuroepithelium through direct interaction with LGN. The Journal of cell biology 206:707-717.

25. Kiyomitsu, T., and I. M. Cheeseman. 2013. Cortical dynein and asymmetric membrane elongation coordinately position the spindle in anaphase. Cell 154:391-402.

26. Woodard, G. E., N. N. Huang, H. Cho, T. Miki, G. G. Tall, and J. H. Kehrl. 2010. Ric-8A and Gi alpha recruit LGN, NuMA, and dynein to the cell cortex to help orient the mitotic spindle. Molecular and cellular biology 30:3519-3530.

27. Zheng, Z., Q. Wan, J. Liu, H. Zhu, X. Chu, and Q. Du. 2013. Evidence for dynein and astral microtubule-mediated cortical release and transport of Galphai/LGN/NuMA complex in mitotic cells. Molecular biology of the cell 24:901-913.

28. Kamath, K., T. Okouneva, G. Larson, D. Panda, L. Wilson, and M. A. Jordan. 2006. 2-Methoxyestradiol suppresses microtubule dynamics and arrests mitosis without depolymerizing microtubules. Molecular cancer therapeutics 5:2225-2233.

29. Kimura, K., and A. Kimura. 2011. A novel mechanism of microtubule length-dependent force to pull centrosomes toward the cell center. Bioarchitecture 1:74-79.

30. Poirier, C. C., Y. X. Zheng, and P. A. Iglesias. 2010. Mitotic Membrane Helps to Focus and Stabilize the Mitotic Spindle. Biophys J 99:3182-3190.

Supplementary Information

Dynamic modelling reveals the separable contributions to achieving correct spindle orientation in a noisy system

Adam M. Corrigan, Roshan Shrestha, Viji M. Draviam and Athene M. Donald

Experimental Protocols

HeLa cells stably expressing tubulin-RFP and histone H2B-GFP were cultured as previously described (1). For imaging, cells were plated into 8-well imaging dishes (Lab-tek, Fisher), and complete DMEM media was replaced with L15 medium prior to imaging. Time-lapse movies were captured in RFP, GFP and DIC channels, for up to 4 hours with a frame interval of 3 minutes, using a DeltaVision Core inverted microscope (Applied Precision). Multiple z-slices were captured to ensure the spindle was continuously observed. Movies were analysed using spindle3D software (1) to extract dynamic measurements. Briefly, spindle pole positions were automatically identified on a frame-by-frame basis, extracted for fast manual verification and used to calculate the spindle orientation over time. Anaphase was marked as the first frame in which separation of daughter chromosomes is detectible.

Simulations were carried out using custom-written code in MATLAB (The Mathworks). Where required, simulated spindle traces were downsampled to the desired imaging interval and analysed in the same manner as the experimental data.

Parameter	Symbol	Value
Activation rate	κ_0	0.0028 s^{-1}
Cue lifetime	τ_{cue}	2 s
Effective cue impulse	f_0	0.028 rad.m^{-1}
Random Noise	σ_0	0.0063 rad.s^{-1}
Total cue number	N	60
Cue order parameter	ρ	0.087
Relative spindle size	a/R	0.6
Simulation timestep	t_{step}	0.2 s

Table I: Parameters used in simulating the standard experimental configuration. Total cue number was selected to be consistent with previous literature, slightly below the value used by Thery et al (2) for cells cultured on artificial fibronectin patterns. Cue order parameter and spindle size calculated from experimental measurements. Cue impulse, activation rate and random noise were found from a parameter space search to give spindle dynamics consistent with experimental measurements (see main text). The simulation timestep was set to be sufficiently short that the spindle position, and therefore the torque and astral microtubule densities, do not change significantly during the time interval. Note that the unusual units for the cue force and noise arise from subsuming the rotational frictional drag coefficient of the spindle into these parameters.

Two Regimes of Spindle Movement

In the initial experimental study(1), it was found that the absolute rate of spindle rotation was reduced by a small amount when the spindle was close to the long axis compared to spindles further

from alignment along the long axis. We denote the mean and standard deviation of the rotation speed by μ_Ω and σ_Ω respectively, approximated by equations A6 and A7 in Appendix B. The absolute rate of rotation differs from μ_Ω in that the absolute rate does not distinguish between clockwise/positive or anti-clockwise/negative directions. However a similar measure, the root-mean-square rotation rate, can be derived from μ_Ω and σ_Ω using the definition of variance:

$$\sigma^2 = \left\langle \Delta\phi^2 \right\rangle - \left\langle \Delta\phi \right\rangle^2$$

$$\sigma_\Omega^2 = \Delta\phi_{RMS}^2 - \mu_\Omega^2$$

$$\Delta\phi_{RMS} = \left[\mu_\Omega(\phi)^2 + \sigma_\Omega^2 \right]^{1/2} \qquad\qquad \text{Eq (S1)}$$

While σ_Ω depends on the total number of cues and varies only weakly with spindle orientation, μ_Ω varies with φ and vanishes at the long axis, meaning the absolute rate of rotation is reduced close to alignment.

The magnitude of the difference between the two regimes depends on the frame interval. Longer frame intervals average the spindle movement over a larger number of contributions, and correspondingly increase the apparent bias in direction and rotation suppression, while shorter frame intervals are more dominated by random behaviour and thus show an apparently decreased bias and a reduced difference between the two regimes of spindle rotation. It is therefore important to consider the frame interval when quoting or comparing rates of rotation. The presence of the two regimes of rotation dynamics is fundamentally linked to the angle-dependent bias in rotation direction. At the higher bias values around 45 degrees from alignment, cue contributions will tend to add together in the same direction, leading to a relatively large overall movement. Close to alignment, when the bias is 0, individual cue contributions are more likely to cancel each other out, summing to give a smaller displacement. Through μ and σ, the suppression ratio, $\Delta\varphi_{RMS}(0°)/\Delta\varphi_{RMS}(45°)$, is influenced by the distribution of cortical cues; more polarised distributions give rise to a greater difference between the two regimes.

Supplementary References

1.   Corrigan, A. M., R. L. Shrestha, I. Zulkipli, N. Hiroi, Y. Liu, N. Tamura, B. Yang, J. Patel, A. Funahashi, A. Donald, and V. M. Draviam. 2013. Automated tracking of mitotic spindle pole positions shows that LGN is required for spindle rotation but not orientation maintenance. Cell cycle 12:2643-2655.
2.   Thery, M., A. Jimenez-Dalmaroni, V. Racine, M. Bornens, and F. Julicher. 2007. Experimental and theoretical study of mitotic spindle orientation. Nature 447:493-U496.
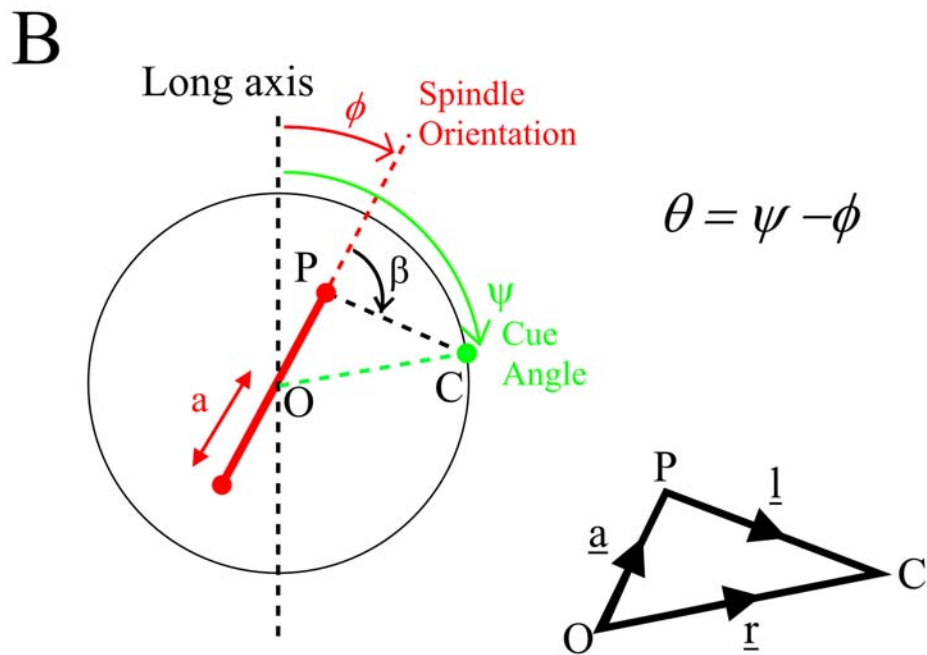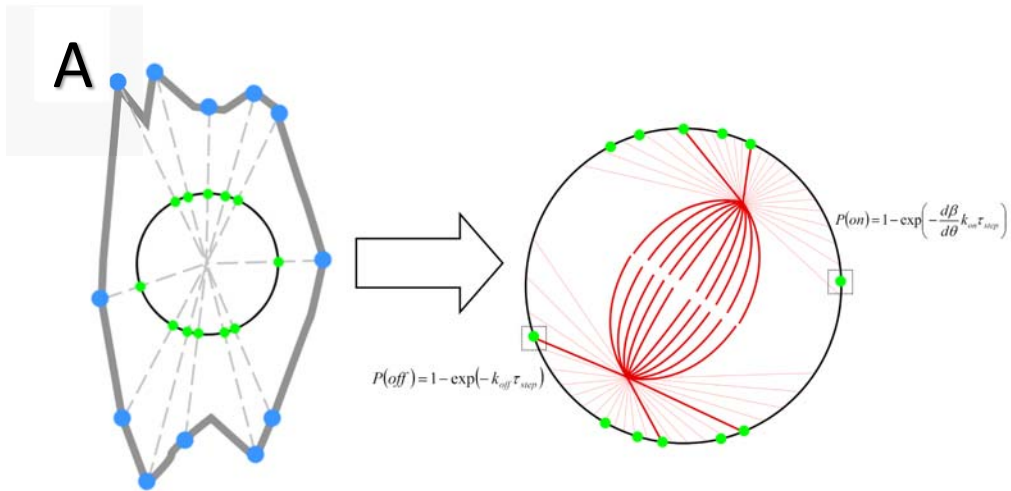
Figure S1 – Geometry of the spindle and rounded mitotic cell. A – Locations of focal adhesions during interphase are converted to angular positions of cortical cues by keeping the angle of the cues from the centre of the cell constant. B – Labelling of variables used in the dynamic model.
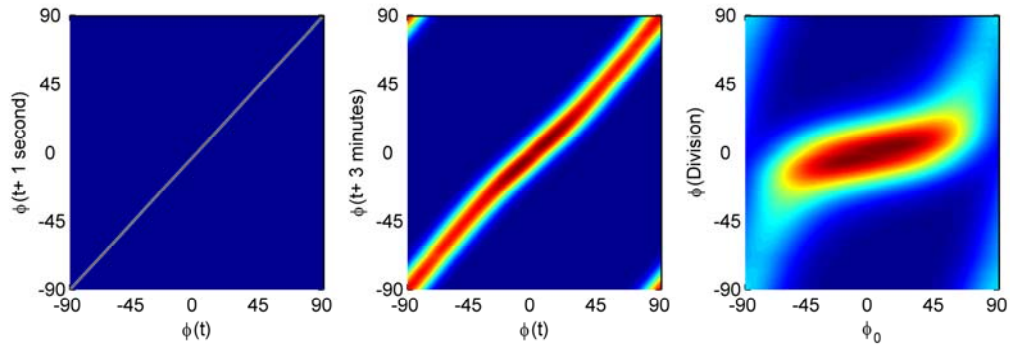
Figure S2 – Stochastic matrix formulation of spindle dynamics. Left – the spindle displacement distribution is calculated over a very short timescale, in this case 1 second, giving stochastic matrix **M₁**. Middle – the behaviour from one frame to the next is given by $\mathbf{M_{frame}} = \mathbf{M_1}^{t_{frame}}$. Right – Probability distribution, $P(\phi_{division}|\phi_0)$, calculated from equation A5 in Appendix A.

Figure S3 – Representative angular cue distributions for the values of the cue order parameter shown. The order parameter represents the strength of anisotropy in the cue distribution, and is used as a proxy for aspect ratio in our model.
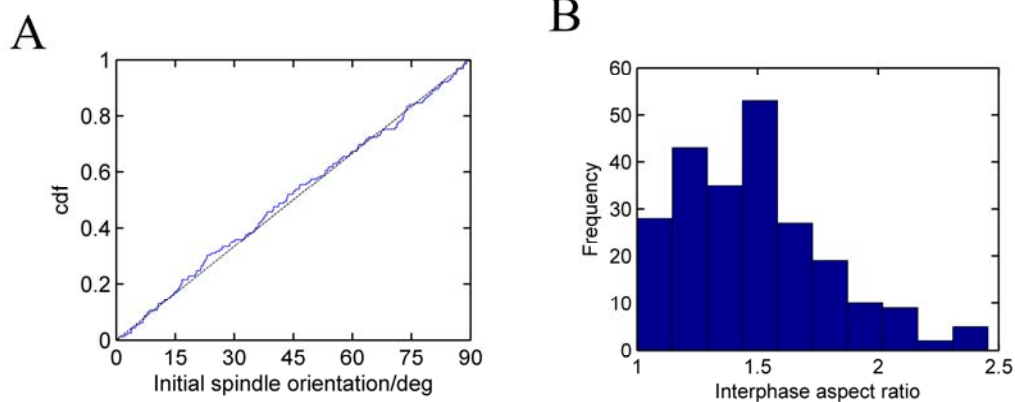
Figure S4 – Summary of experimental dynamic behaviour. A – Cumulative distribution of initial orientation upon spindle formation (solid blue line) compared with uniform distribution (dotted line). B – Distribution of aspect ratio measurements of cell shape, measured 15 minutes before NEBD.
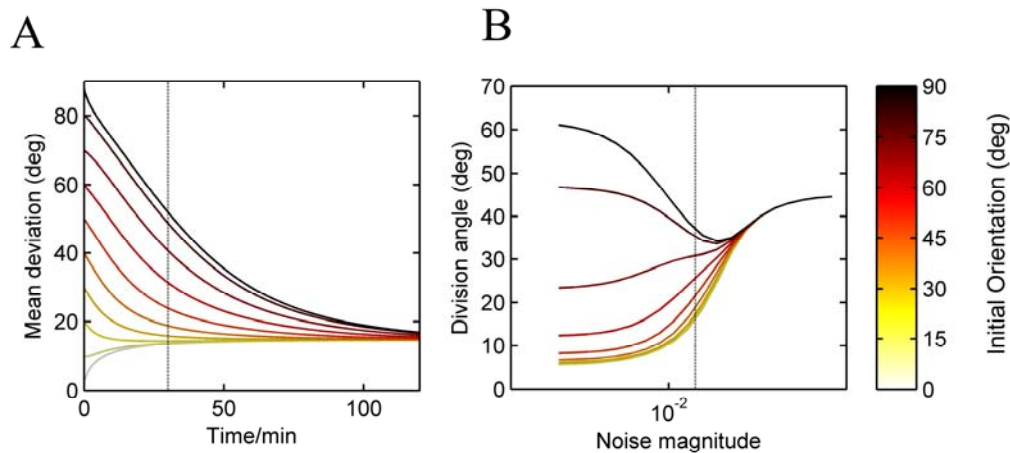
Figure S5 – Initial orientation and alignment success. A – Average spindle deviation from the long axis as a function of time after NEBD, for different starting orientations. The vertical dashed line denotes the typical experimental mitosis duration. B – Average final spindle deviation upon anaphase onset, as the noise magnitude is varied, for different starting orientations. The dashed line indicates the magnitude of noise used in the standard control configuration. Reducing the noise below this value reduces the degree of alignment for spindles which begin far from alignment, without greatly improving the alignment of other spindles. In A and B, line colour denotes initial orientation.